Available online at www.sciencedirect.com
ScienceDirect
Thermochimica Acta 449 (2006) 8–15
thermochimica acta
www.elsevier.com/locate/tca

Reaction rate coefficients in decomposition of lumpy limestone of different origin

Chuan Cheng*, Eckehard Specht

Faculty of Process and Systems Engineering, Magdeburg University, D-39106 Magdeburg, Germany

Received 31 January 2006; received in revised form 20 April 2006; accepted 5 June 2006
Available online 12 June 2006

Abstract

A method is described to evaluate the reaction rate coefficients, pore diffusivity and thermal conductivity of the lime layer in the decomposition of limestone by linearization of conversion curves, based on the shrinking core model. Spherical and long cylindrical samples with diameters in the range of 20–50 mm were prepared and thermally decomposed in a chamber furnace at constant temperature and CO_2 pressure. By weighing and simultaneous measuring of the internal temperature, the decomposition behavior of these samples was studied. The reaction rate coefficients thus obtained vary from 0.003 to 0.012 m s^{-1} with a factor of 4, depending upon the origin of the limestone. The reaction coefficients measured by other authors based on limestone powder lie within this range.

Keywords: Limestone decomposition; Reaction rate coefficient; Pore diffusivity; Thermal conductivity

1. Introduction

Limestone ($CaCO_3$) is an important natural raw material in many branches of industry. Before final utilization, a large part of limestone must be calcined in shaft or rotary kilns, where carbonate is thermally decomposed, splitting off CO_2 and yielding quicklime, which can be used, for example, in construction, in metallurgy, and as a flue gas desulphurizing agent.

The endothermic decomposition consists of five subprocesses: heat transfer from the ambient to the solid surface, heat conduction from the surface to the reaction front, chemical reaction at the front, diffusion of CO_2 through the porous oxide layer to the surface, and then mass transfer into the surroundings. The heat and mass transfer between fluid and solids have already been adequately investigated for flows around individual bodies and in chemical apparatus such as, for example, packed beds. In most books on heat transfer, e.g. [1], the equations are given. However, it is difficult to measure the reaction rate coefficient, the thermal conductivity and the pore diffusivity of CO_2 in the lime layer during calcination.

Nearly all researchers have studied the reaction kinetics of limestone decomposition, using limestone particles in millimeter or micrometer range to exclude the influence of thermal conduction, pore diffusion, heat and mass transfer. Ingraham and Marier [2] have taken 6.4 mm pellets of reagent $CaCO_3$ and obtained a rate coefficient of 0.015 mol m^{-2} s^{-1} at 850 °C. Borgwadt [3] measured two types of limestone based on 1 μm powder, and concluded that the rate coefficient at 850 °C is 0.012 mol m^{-2} s^{-1}. Fuertes et al. [4] conducted experiments over a size range of 0.25–1.85 mm in a fluidized bed. Their result was 0.077 mol m^{-2} s^{-1} at 850 °C. Using a thermogravimetric analyzer under non-isothermal conditions, Rao [5] studied powders with an average grain size of 10.7 μm. A reaction rate of 0.054 mol m^{-2} s^{-1} at 850 °C can be calculated from his equations. Under different total pressure, Garcia-Labiano et al. [6] experimented on limestone particles between 0.4 and 2 mm with a thermogravimetric analyzer. From their data of sample Blanca a reaction rate of 0.128 mol m^{-2} s^{-1} at 850 °C can be obtained. Ar and Dogu [7] investigated thermogravimetrically some samples with average size of 1 mm, from Turkey, and their rate coefficients at 850 °C were about 0.075 mol m^{-2} s^{-1}.

In the above researches, the values of reaction rate coefficient fluctuate with a factor of 6. In this study the decomposition of different types of limestone are investigated to see whether

* Corresponding author. Tel.: +49 391 6711318; fax: +49 391 6712762.
E-mail address: chengchuan@web.de (C. Cheng).

0040-6031/$ – see front matter © 2006 Elsevier B.V. All rights reserved.
doi:10.1016/j.tca.2006.06.001

Nomenclature

A	area (m^2)
b	shape factor
D^P	effective pore diffusivity ($m^2\,s^{-1}$)
f	form function
k	reaction rate coefficient in Eq. (3) ($m\,s^{-1}$)
k_1	reaction rate coefficient in Eq. (19) ($mol\,m^{-2}\,s^{-1}$)
K_C	volume concentration of CO_2 in carbonate ($kg\,m^{-3}$)
$\dot{m}$	mass flux ($kg\,m^{-2}\,s^{-1}$)
M	mass (kg)
P	pressure (Pa)
P^*	equilibrium pressure (Pa)
$\dot{q}$	heat flux ($J\,m^{-2}\,s^{-1}$)
r	position coordinate, radius (m)
R	general gas constant ($J\,mol^{-1}\,K^{-1}$)
R_C	special gas constant of CO_2 ($J\,kg^{-1}\,K^{-1}$)
R_i	resistance of sub-process (s)
t	time (s)
T	temperature (K)
X	conversion degree

Greek symbols

α	heat transfer coefficient ($W\,m^{-2}$)
β	mass transfer coefficient ($m\,s^{-1}$)
Δh_R	specific reaction enthalpy ($J\,kg^{-1}$)
ΔH_R	reaction enthalpy ($J\,mol^{-1}$)
λ	thermal conductivity ($W\,m^{-1}\,K^{-1}$)

Subscripts

A	ambient
C	CO_2
D	diffusion
F	reaction front
k	chemical reaction
M	core, center
MAX	maximum
OX	oxide
R	reaction
S	surface
α	heat transfer
β	mass transfer
λ	heat conduction

Superscript

*	equilibrium
P	pore

the reaction depends on the origin. In industry lumpy limestone pieces of centimeters are usually burnt. Therefore the experiments were conducted using lumpy pieces with defined shapes to see whether the value obtained from grains can also be applied to lumpy pieces.

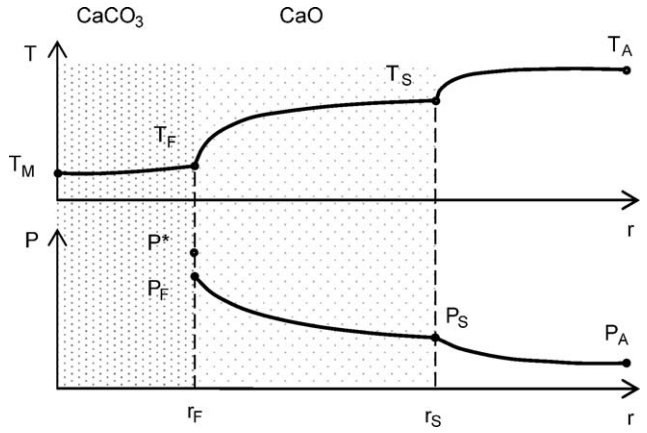

Fig. 1. Model of limestone decomposition.

2. Decomposition model of limestone

The decomposition of limestone is an endothermic topochemical reaction:

$$\underset{\text{(solid)}}{CaCO_3} + \underset{\text{(reaction enthalpy)}}{\Delta H_R} = \underset{\text{(solid)}}{CaO} + \underset{\text{(gaseous)}}{CO_2}$$

The calcination process can be explained using a partially decomposed piece of carbonate, whose profiles of CO_2 partial pressure and temperature are shown in Fig. 1. The specimen comprises a dense carbonate core surrounded by a porous oxide layer. In the calcination reactor at temperature T_A heat is transferred by radiation and convection (symbolized by α) to the solid surface at a temperature of T_S. By means of thermal conduction (λ) heat penetrates through the porous oxide layer at an average temperature of T_{OX} to reach the reaction front, where the temperature is T_F. As the reaction enthalpy is many times greater than the internal energy, the heat flowing further into the core is negligible during reaction. Therefore the core temperature is only slightly lower than the front temperature. Once heat is supplied, the chemical reaction (k) then takes place, for which the driving force is the deviation of CO_2 partial pressure from the equilibrium ($P^* - P_F$). The released CO_2 diffuses (D^P) through the porous oxide layer to the surface and finally passes by convection (β) to the surroundings where the CO_2 partial pressure P_A exists.

The four physical transport processes and the chemical kinetics involved are therefore interconnected. The resistances caused by heat transfer, heat conduction, chemical kinetics, pore diffusion and mass transfer can be understood with analog to serial electrical resistances, R_α, R_λ, R_k, R_D and R_β, in causal sequence.

A one-dimensional shrinking core model can be established based on the assumptions of ideal sample geometry such as sphere, cylinder or plate, a homogeneous chemical composition and structure in the sample, and a symmetrical heat supply. The reaction starts uniformly on the solid surface, always forming a smooth reaction front, which then advances continuously into the interior. This fact has been partly proven with SEM (scanning electron microscopic) by Fuertes et al. [4] and Rähder [8]. The edges of the individual crystals are the preferred locations where the reaction starts. Therefore the actual reaction surface

is, as demonstrated by Fuertes et al. [4], somewhat larger than the assumed smooth surface. This deviation has been incorporated in the reaction rate coefficient in this research.

Based on the shrinking core model, Szekely et al. [9] and Kainer et al. [10] have derived analytical equations to calculate the decomposition of spherical and cylindrical limestone pieces. Assuming a pseudo steady state and constant material properties, Eq. (1) is obtained (for spherical geometry, for example) by combining the heat transfer at the particle surface and the heat conduction in the lime layer:

$$\dot{q} = \frac{\lambda}{r_F^2\left(\frac{1}{r_F} - \frac{1}{r_S} + \frac{\lambda}{\alpha r_S^2}\right)}(T_A - T_F), \tag{1}$$

where α accounts for both the convection and the radiation heat transfer.

Similarly, Eq. (2) is derived (for spherical geometry, for example) by combining the mass transfer of CO_2 at the particle surface and the diffusion in the lime layer:

$$\dot{m} = \frac{D^P}{r_F^2\left(\frac{1}{r_F} - \frac{1}{r_S} + \frac{D^P}{\beta r_S^2}\right)}\frac{1}{R_C}\left(\frac{P_F}{T_F} - \frac{P_A}{T_A}\right). \tag{2}$$

For the reaction at the front, the reaction rate is proportional to the deviation of partial pressure from equilibrium, $P^* - P_F$:

$$\dot{m} = \frac{k}{R_C T_F}(P^* - P_F). \tag{3}$$

The heat flux and mass flux are related by

$$\dot{q} = \Delta h_R \dot{m}, \tag{4}$$

where Δh_R is the specific reaction enthalpy corresponding to the produced CO_2 in mass, 3820 kJ kg^{-1}.

The mass flux of CO_2 is expressed as

$$\dot{m} = -K_C\frac{dr_F}{dt}, \tag{5}$$

where K_C is the concentration of CO_2 in limestone, e.g. 1190 kg CO_2 m^{-3} for a pure limestone with a density of about 2700 kg m^{-3}.

The conversion degree X is calculated by

$$X = \frac{M}{M_{t=0}} = 1 - \left(\frac{r_F}{r_S}\right)^b, \tag{6}$$

where the shape factor $b = 1$, 2 or 3 for a plate, cylinder or sphere, respectively.

Two coupled differential equations for the conversion degree and the decomposition temperature can be then derived from the above system:

$$\frac{dX}{dt}[R_\alpha + R_\lambda f_1(X)] = 1, \tag{7}$$

$$\frac{dX}{dt}[R_\beta + R_D f_1(X) + R_k f_2(X)] = 1, \tag{8}$$

where the form functions $f_1(X)$ and $f_2(X)$ are summarized in Table 1. The resistances R_i, where T_F is included, are given in Eqs. (9)–(13):

$$R_\alpha = \frac{K_C \Delta h_R}{T_A - T_F}\frac{r_S}{\alpha b}, \tag{9}$$

$$R_\lambda = \frac{K_C \Delta h_R}{T_A - T_F}\frac{r_S^2}{2\lambda b}, \tag{10}$$

$$R_k = \frac{K_C R_C T_F}{P^* - P_A}\frac{r_S}{k}, \tag{11}$$

$$R_D = \frac{K_C R_C T_F}{P^* - P_A}\frac{r_S^2}{2D^P b}, \tag{12}$$

$$R_\beta = \frac{K_C R_C T_F}{P^* - P_A}\frac{r_S}{\beta b}. \tag{13}$$

To supplement the above equation system, the dependence of equilibrium pressure upon the temperature is described thermodynamically by

$$P^* = P^*_{MAX}\exp\left(-\frac{\Delta H_R}{RT_F}\right), \tag{14}$$

where P^*_{MAX} is 4×10^7 bar and ΔH_R is 168 kJ mol^{-1}. There is no discernible dependence of the equilibrium pressure upon the genesis and nature of the limestone concerned.

With Eqs. (7)–(14), X and T_F can be calculated as functions of time t.

3. Evaluation method

In experiments, to be demonstrated later, it will be shown that the temperature at the reaction front T_F changes only slightly during decomposition under constant ambient conditions (P_A and T_A), especially when $0.1 < X < 0.9$. Therefore the corresponding equilibrium pressure P^* and resistances R_i remain virtually constant during decomposition. Taking T_F as constant, an analytical

Table 1
Form functions for different geometries

	Plate	Cylinder	Sphere
$f_1(X)$	$f_1(X) = 2X$	$f_1(X) = 2X\ln(1-X)^{-1/3}$	$f_1(X) = 2[(1-X)^{-1/3} - 1]$
$f_2(X)$	$f_2(A) = 1$	$f_2(A) = (1/2)(1-X)^{-1/2}$	$f_2(A) = (1/3)(1-X)^{-2/3}$
$f_3(X)$		$f_3(X) = X$	
$f_4(X)$	$f_4(X) = X^2$	$f_4(X) = (2/3)[X + (1-X)\ln(1-X)]$	$f_4(X) = 3[1-(1-X)^{2/3}] - 2X$
$f_5(X)$	$f_5(X) = X$	$f_5(X) = 1-(1-X)^{1/2}$	$f_5(X) = 1-(1-X)^{1/3}$

solution of this system can be achieved by integrating Eqs. (7) and (8):

$$t = R_\alpha f_3(X) + R_\lambda f_4(X), \tag{15}$$

$$t = R_\beta f_3(X) + R_D f_4(X) + R_k f_5(X), \tag{16}$$

where the form functions $f_3(X)$, $f_4(X)$ and $f_5(X)$ are summarized in Table 1 as well.

Given an experimentally determined decomposition progress and measured T_F, the desired material properties (λ, D^P and k) can be derived. Eqs. (15) and (16) can be transformed into two linear equations:

$$\frac{t}{f_3(X)} = R_\alpha + R_\lambda \frac{f_4(X)}{f_3(X)}, \tag{17}$$

$$\frac{t - R_\beta f_3(X)}{f_5(X)} = R_k + R_D \frac{f_4(X)}{f_5(X)}. \tag{18}$$

The resistance R_β, which is usually very small compared with the other four, can be calculated separately and can therefore be presumed to be known. Then R_α, R_k, R_λ and R_D can be easily obtained from the intercepts and slopes. Similar linearized equations can be derived if Eqs. (15) and (16) are divided by $f_4(X)$ instead of by $f_3(X)$ and $f_5(X)$. However, Eqs. (17) and (18) are more convenient for evaluation. Finally, the required material properties (λ, D^P and k) can then be determined from Eqs. (10)–(12).

The experimental determination of desired values requires constant ambient conditions and measurement of time-dependent progress of the conversion degree (by weighing, for example) and the front temperature (by thermal couples, for example).

4. Experimental apparatus

The evaluation of the above equations requires particles of cylindrical or spherical shape. Cylinders were prepared from large limestone pieces using hollow drillers. From some of these cylinders spheres were drilled. The experimental apparatus for measuring the decomposition behavior is shown schematically in Fig. 2.

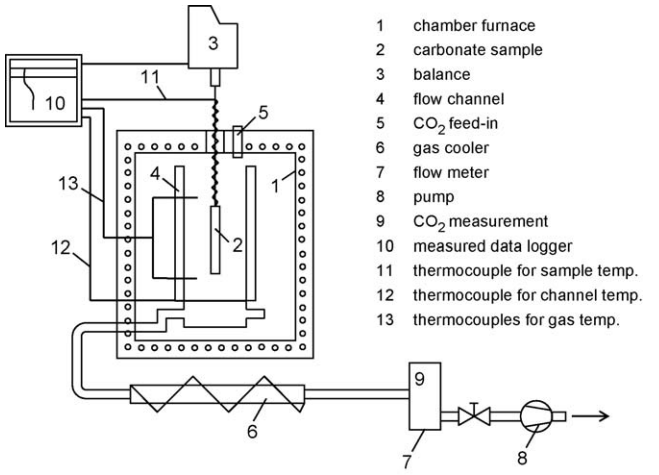

Fig. 2. Experimental apparatus for measuring limestone decomposition.

The limestone specimens were suspended from a balance with which the weight loss and therefore the conversion degree could be recorded continuously. In order to have well-defined flow conditions around the specimen and to be able to determine the convective heat and mass transfer, the specimen was enclosed within a cylindrical flow channel mounted in an electrically heated chamber furnace whose temperature was kept constant. Hot gas was introduced at the top of the channel and sucked off at a defined rate from the bottom. This prevented an enrichment of CO_2 in the channel, so that the ambient partial pressure of CO_2 was kept constant. In the center of the specimen small holes were drilled. The temperatures inside the specimen were measured by thermocouples inserted in the holes. These were mounted at the center for all the specimens involved, and also at the periphery for some specimen. The wall temperature of the channel was measured at various positions with thermocouples, whose measurements showed that the channel had a uniform temperature. An infrared absorption gas analyzer continuously indicated the concentration of CO_2.

Table 2
Chemical composition (%) and bulk density of the types of limestone investigated

	Cretaceous limestone		Jurassic limestone		Devonian limestone			Marble
	Laegerdorf	Langelsheim	Regensburg	Blaustein	Winterberg	Stromberg	Diez	Cercos
CaO	54.240	52.47	55.11	55.70	54.29	55.41	55.510	55.34
MgO	0.260	0.30	0.400	0.190	0.39	0.43	0.400	0.59
SiO_2	1.860	4.68	0.340	0.240	1.83	0.26	0.100	0.08
Fe_2O_3	0.080	0.24	0.090	0.032	0.21	0.06	0.010	0.05
Al_2O_3	0.27	0.63	0.12	0.043	0.08	0.13	0.013	0.01
K_2O	0.046	0.08	0.017	0.007	0.02	–	0.005	0.004
Na_2O	0.041	0.03	0.018	0.013	0.01	–	0.013	0.01
BaO	0.01	0.01	0.011	0.012	0.02	–	0.008	0.01
SrO	0.036	0.03	0.005	0.004	0.02	–	0.009	0.01
Mn_XO_Y	0.016	0.03	0.024	0.013	0.02	0.02	0.011	0.004
SO_3	0.055	0.05	0.043	–	0	–	–	–
Weight loss	42.81	41.50	43.62	43.51	43.05	43.78	43.540	43.97
Sum.	99.720	100.06	99.80	99.76	99.94	100.09	99.64	100.08
Density (g cm^{-3})	1.57	2.51	2.68	2.61	2.68	2.69	2.70	2.71

The tests were performed using spheres with diameters of 25 and 46 mm, and cylinders with diameters of 20, 25 and 46 mm. The length/diameter ratios of the cylinders ranged from 5 to 12, so that they could be regarded as infinitely long and treated as one-dimensional cases.

The chemical composition of the limestone investigated is given in Table 2.

5. Decomposition behavior

The decomposition behaviors recorded experimentally were similar for both spherical and long cylindrical samples. In both cases the front temperatures stayed nearly constant. Using different form functions in Table 1, the same linearized decomposition diagrams could be plotted. But for the purpose of material property evaluation, cylindrical geometry had advantage because the samples were easier to prepare. When the length/diameter ratio of cylinder was greater than 5, no more discernible influence of it could be observed. The volume of sample, as well as the ambient temperature, affected the front temperature. Because of larger resistance for heat supply a bigger specimen demonstrated a smaller reaction velocity, therefore a lower front temperature. In the evaluation, however, the conversion curves could be linearized satisfactorily, independent of the front temperature.

As an example, Fig. 3 shows typical curves of X and T_F for two cylindrical limestone specimens with a diameter of 47 mm at different ambient temperatures of 1000 and 910 °C. At temperatures below 750 °C, the equilibrium pressure was so low that no substantial decomposition occurred. The heat supplied was first used only for raising the internal energy of the specimen. In comparison with the total decomposition time the heating-up of the specimen occurred very rapidly. After the heating-up of the specimen had been accomplished, the equilibrium pressure and the decomposition rate became so great that the heat transported to the specimen was consumed virtually only by reaction. The temperature in the carbonate core was then nearly uniform. Only within the oxide layer did the temperature become higher towards the surface. When several thermocouples were positioned at different locations inside the specimen, the progress of the reaction front could be observed. Once the reaction front passed the measuring point, the temperature underwent a significant increase. After completion of decomposition the core temperature finally rose until the ambient temperature was reached and a steady state was established.

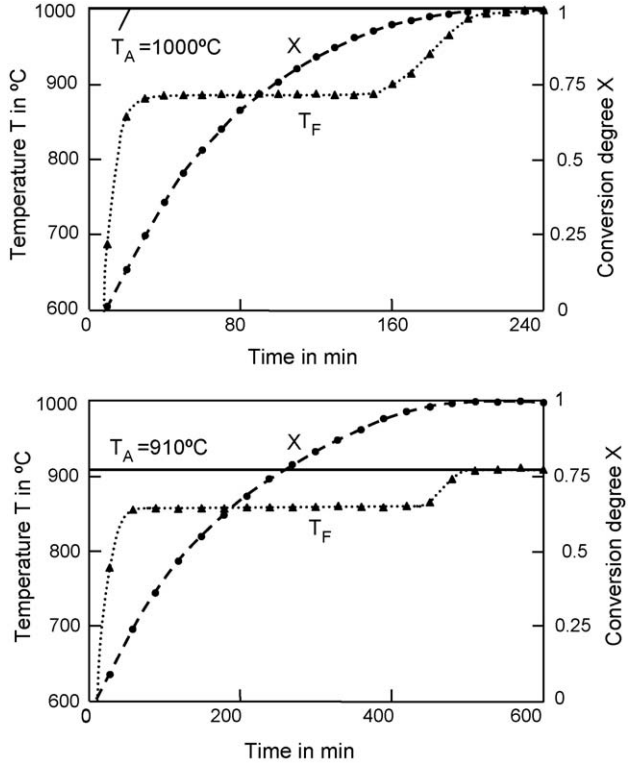

Fig. 3. Typical conversion curves.

The measured conversion curves for the decomposition degree were linearized in accordance with Eqs. (17) and (18). As an example, Fig. 4 shows such diagrams for a cylindrical specimen (diameter 20 mm and length 100 mm) made of limestone from Winterberg. It is obvious that the measured values can be satisfactorily approximated by straight lines, and thus in turn confirms the validity of the equations established above. From the ordinate intercept the reaction rate coefficient and the overall heat transfer coefficient can be determined using Eqs. (11) and (9), respectively, and from the slopes the effective pore diffusivity and the thermal conductivity can be calculated using Eqs. (12) and (10), respectively. The overall heat transfer coefficient in the experimental apparatus is of no further interest. The other three values will now be discussed.

6. Material values

6.1. Reaction rate coefficients

The reaction rate coefficients determined from the linearized conversion curves are represented in Fig. 5. It is obvious that they are not strongly, if at all, dependent on the temperature. The main dependence of the decomposition time on the temperature is therefore due to the exponential temperature dependence of the equilibrium pressure. There is also no ascertainable influence of the CO_2 partial pressure on the reaction coefficient. It may further be shown that the reaction rate coefficient of the limestone investigated depends more on its type than its geographical origin. Jurassic limestone has the lowest reaction rate coefficients, cretaceous limestone the highest and Devonian limestone is somewhere between the two. The reaction rate coefficient averages 0.005 m s^{-1}, ranging from 0.003 to 0.012 m s^{-1}, that is to say, with a factor of 4.

In the literature the reaction rate coefficient is defined differently, with different dimensions. Most authors assumed the expressions of reaction kinetics in [11]:

$$\dot{N} = k_1 A_F \left(1 - \frac{P_F}{P^*}\right), \tag{19}$$

where $\dot{N}$ is the molar flow rate of produced CO_2, mol m^{-2} s^{-1}.

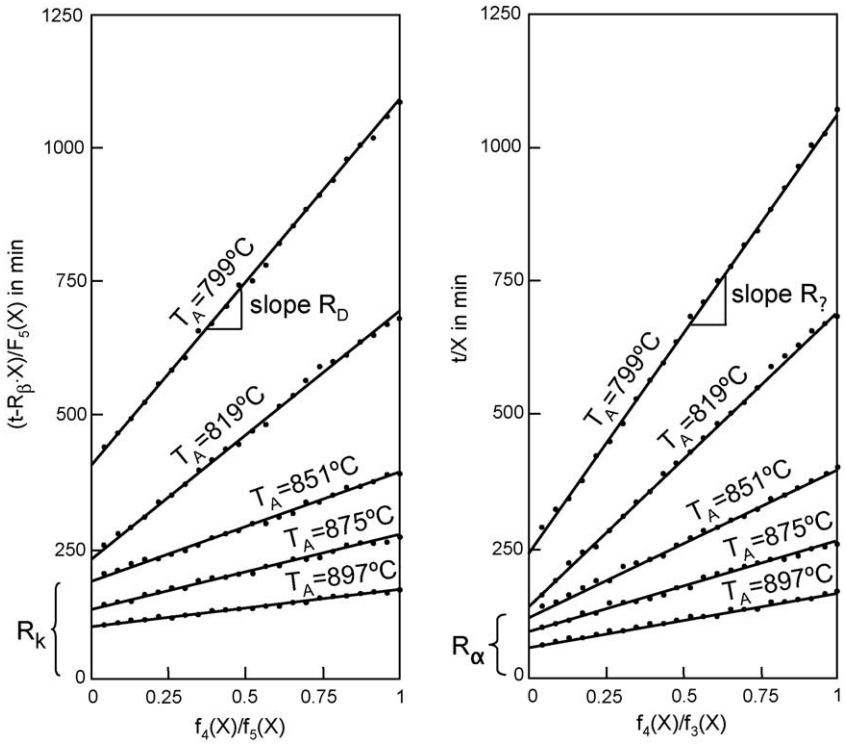

Fig. 4. Linearized decomposition diagrams.

For comparison, the reaction rate coefficient k expressed in Eq. (3) can be converted to k_1 in Eq. (19) by

$$k_1 = \frac{kP^*}{RT_F}. \quad (20)$$

Values thus converted are represented in Fig. 6 as well.

Using the definition in Eq. (19), Ingraham and Marier [2] examined the decomposition of 6.4 mm pellets of reagent $CaCO_3$ in air. Borgwadt [3] measured the reaction rate of limestone particles ranging in size from 1 to 90 μm, over the temperature range from 516 to 1000 °C. He used two naturally occurring types of limestone, representing markedly different physical and geological properties. One stone is Fredonia Valley White, and the other is Georgia Marble. Fuertes et al. [4] studied the decomposition of limestone particles, ranging in size from 0.25 to 1.85 mm, in a fluidized bed, over temperatures between 1034 and 1173 K, at different CO_2 concentrations from 0 to 15%. His samples came from Riosa, Asturias, Spain. Rao [5] carried out exper-

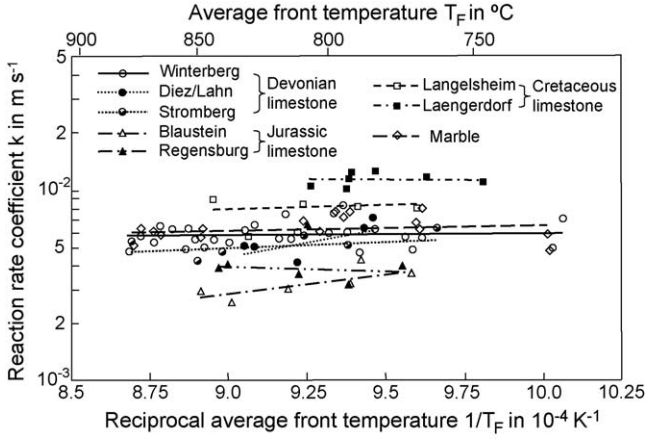

Fig. 5. Reaction rate coefficients of various types of limestone.

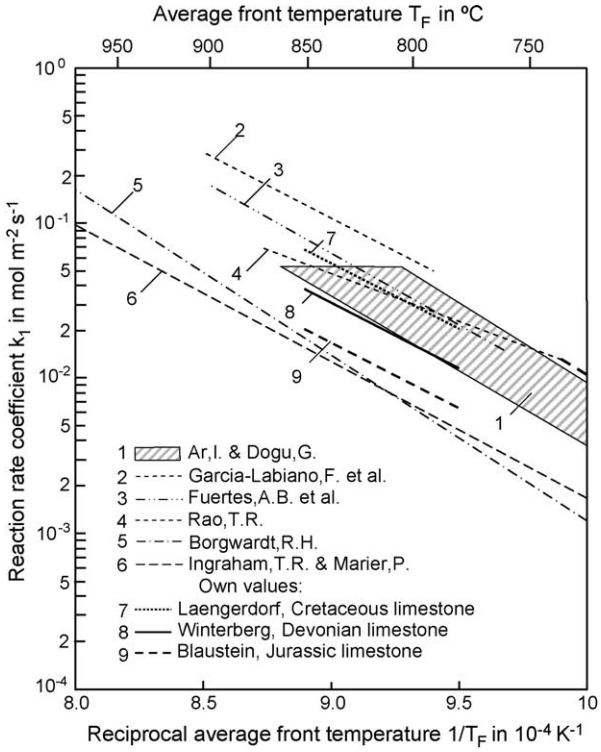

Fig. 6. Reaction rate coefficients comparison.

iments with a thermogravimetric analyzer under non-isothermal conditions with different heating rates (10–100 K min^{-1}). His sample was Analar grade calcium carbonate (May and Bakerm Ltd., Dagenham, England), with an average grain size of 10.7 μm. Considering CO_2 adsorption on the reaction interface under different total pressure, Garcia-Labiano et al. [6] used a similar definition to evaluate the decomposition kinetics of limestone sample Blanca with a size between 0.4 and 2 mm, in a temperature range from 1048 to 1173 K. Ar and Dogu [7] investigated the calcination reaction of 10 different samples with average size of 1 mm, which were taken from different regions of Turkey, using thermogravimetric analysis. Their values of reaction rate coefficients are summarized in Fig. 6.

It is clear that the values obtained by the above-mentioned authors are within the range of our results, irrespective of grain size. This indicates that the variation of reaction rate coefficients in previous works can probably be explained by different types or origins of limestone rather than the possible difference in methods or experimental errors.

6.2. *Effective pore diffusivity*

The effective pore diffusivity determined from the slope of the linearized decomposition diagrams in Fig. 4 is represented in Fig. 7. The effective pore diffusivity varies with sample origin with a factor of 10. It has considerable temperature dependence as well.

The magnitude of the pore diffusivity is substantially determined by the developed pore structure. Immediately after the decomposition, the pore size distribution in the formed oxide was measured with a mercury porosimeter with a pressure range of 0–2000 bar. The values of the mean diameter were in the range of 0.1–1 μm, which were smaller than the free path length of CO_2. The higher the temperature in the oxide layer was, the stronger was the sintering effect, which resulted in a larger pore

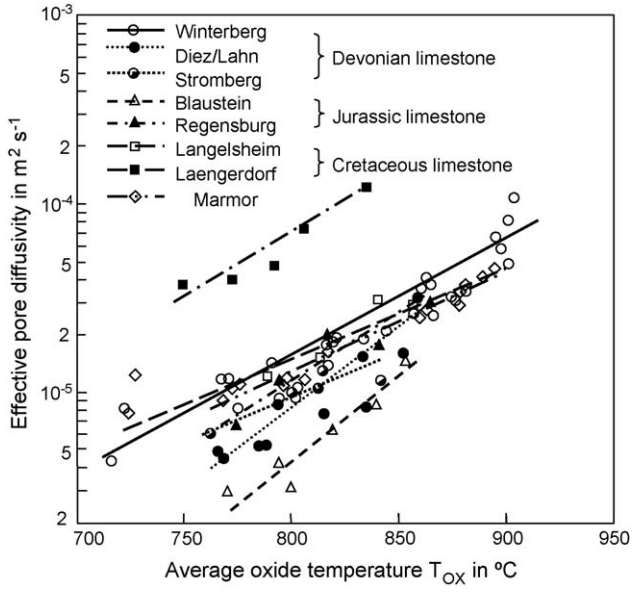

Fig. 7. Temperature dependence of effective pore diffusivity.

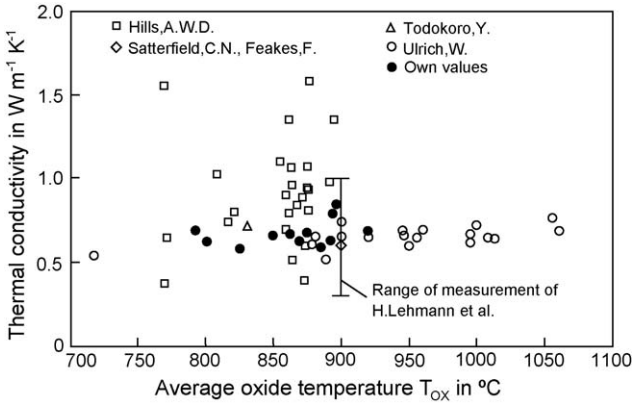

Fig. 8. Thermal conductivity of lime layer.

size and a smaller specific surface. The pore size depended both on the origin of the limestone and on the temperature at which the decomposition took place. Hence the transport of CO_2 through the oxide took place entirely by Knudsen diffusion, and the diffusivity was proportional to the pore diameter.

6.3. *Thermal conductivity*

Similarly, the thermal conductivity was estimated from the slope of the linearized conversion curve in Fig. 4. The values were in the range of 0.55–0.85 W m^{-1} K^{-1}. The thermal conductivity here demonstrated no discernible dependence on temperature or material.

In Fig. 8 our results are compared with some values from the literature, using special direct measurement methods. Both values lie in the same range, which demonstrates that our evaluation method is reliable.

7. Conclusions

Lumpy limestone specimens of long cylindrical and spherical shapes and of 10 different origins were decomposed under constant ambient conditions. The material properties of lime can be evaluated with the method described above, even when all five sub-processes influence decomposition. This method requires a defined geometry of sample, namely spherical or long cylindrical shapes, and constant ambient conditions. The weight loss must be recorded simultaneously with the core temperature, which is assumed to be the same as the temperature at the reaction front. From the slopes and the ordinate intercepts of linearized conversion curves, the reaction rate coefficient, the effective pore diffusivity and the thermal conductivity can be determined.

The reaction rate coefficient defined in Eq. (3) varies with a factor of 4 and averages 0.005 m s^{-1}. This result is consistent with results published in previous literature, in which fine limestone powders were examined. In these studies, these coefficients also vary roughly in this range and with a factor of about 6. This indicates that the variation of reaction rate coefficients with different types or origins of limestone can be explained by the crystal structure of limestone.

The effective pore diffusivity of produced lime varies with the origin of limestone with a factor of 10. It has a strong dependence on temperature because higher temperature causes sintering of lime and enlarges the pore size. The thermal conductivity of nascent lime is between 0.55 and 0.85 $W\,m^{-1}\,K^{-1}$ without any discernible temperature or material dependence.

References

[1] A.F. Mills, Basic Heat Mass Transfer, Prentice Hall, 1999.
[2] T.R. Ingraham, P. Marier, Can. J. Chem. Eng. 41 (1963) 170.
[3] R.H. Borgwadt, Ind. Eng. Chem. Res. 28 (1989) 493.
[4] A.B. Fuertes, G. Marban, F. Rubiera, Trans. IChemE. 71 (1993) 421–428.
[5] T.R. Rao, Chem. Eng. Technol. 19 (1996) 373–377.
[6] F. Garcia-Labiano, A. Abad, L.F. de Diego, P. Gayan, J. Adanez, Chem. Eng. Sci. 57 (2002) 2381–2393.
[7] I. Ar, G. Dogu, Chem. Eng. J. 83 (2001) 131–137.
[8] M. Rähder, Zur Erzeugung von aktivem Branntkalk, Dissertation TU Clausthal, 1977.
[9] J. Szekely, J.W. Evans, H.Y. Sohn, Gas–Solid-Reactions, Academic Press, New York, 1976.
[10] H. Kainer, E. Specht, R. Jeschar, Cem. Lime Gypsum 39 (1986) 214–219.
[11] J. Zawadski, S. Bretsznajder, Trans. Faraday Soc. 34 (1983) 951.